Random Sampling with Iterative Recovery for Millimeter-Wave Imaging Systems

Hojatollah Zamani, Mohammad Fakharzadeh, *Senior Member, IEEE*, Arash Amini, *Senior Member, IEEE*, and Farokh Marvasti, *Senior Member, IEEE*

Abstract—In this paper, an imaging methodology for mono-static millimeter-wave systems is introduced. When the measured object hologram is piece-wise smooth with sharp boundaries, both low-pass and high-pass components are present in a transform domain. Nevertheless, the edges are sparse in transform domain with respect to the image dimensions. It is shown that the down-sampling of the hologram with an appropriate rate determined by the sparsity level, includes the adequate information of all components for image reconstruction. Using random samples, an algorithm is proposed to recover all the sparse components, iteratively. Simulation results illustrate that a high-resolution recovery can be achieved. For instance, by using 20% of the randomly selected hologram samples, an image recovery with a PSNR of 20 dB is achieved and the object scan time is significantly reduced. The proposed methodology is applied to a practical imaging system operating at 30 GHz, where the results illustrate a successful reconstruction of the images.

Index Terms—Iterative recovery, millimeter wave imaging, mono-static, random sampling.

I. INTRODUCTION

Millimeter-wave imaging systems are widely used for different applications, such as concealed weapon detection (CWD), radar imaging for flaw detection, assisting driving or flying in foul weather, and non-destructive tests [1], [2]. Millimeter-waves naturally pass through the regular thin dielectric material, such as cloth, wood, and plastic. Thus, they are best suited for detection of denser materials such as metals, which reflect the wave. Interestingly, the image resolution of $\sim 1 - 10$ mm, which is necessary for the detection of such objects is achieved in this band. The millimeter-wave imaging systems are categorized into multi-static and mono-static classes. A multi-static system consists of multiple transmitters and receivers in different locations, where the transmitter antennas are turned on sequentially, while the receiving antennas measure the incoming wave simultaneously. In a mono-static system, a transmitter antenna and a receiver antenna are placed at the same location. One of the most conventional imaging methods in mono-static systems is the based on uniform scanning the object area by a transceiver pair in half-wavelength steps to avoid aliasing [3]. Depending on the object size, different number of hologram samples are required in a uniform scan. For instance, for a full human body scan (~ 2 m), about 400 samples are required at 30 GHz ($\lambda \sim 1$ cm). However, most of the images are sparse in a transform domain. Therefore, the number of samples required for a high-quality image reconstruction can be substantially lower than that of the uniform sampling.

Authors are with the EE Department, Sharif University of Technology, Tehran, Iran.(Emails: hojatollah.zamani@ee.sharif.edu, {fakharzadeh, aamini, marvasti}@sharif.edu)

There are different strategies to reduce the number of samples. For instance, a nonuniform structure of linear arrays is designed in [4] to minimize the redundancy of linear arrays. A sparse sampling technique is introduced in [5], where two column arrays, one for TX and one for RX, are used with electronically switching antenna elements. In [6], the data redundancy in a multi-static imaging systems is studied. It is shown that the undesired distortion in reconstructed images can be compensated by applying the modified SAR back-projection algorithm. An array design called 1.5-D sparse is introduced in [7], where the elements positions are determined by applying a row-wise orthogonality constraint to gain from the diversity of information.

Sparsity is a fundamental property in the reconstruction of images. For sparse images, the number of required samples to reconstruct the image can reach values far below the Nyquist rate. Theoretically, the number of required samples for the perfect reconstruction is twice the sparsity number (the number of non-zero coefficients in the sparse domain) and not twice the length of an interval that contains all non-zero coefficients [8]. There are two main categories of sparse images [9]. In the first category, the images are sparse in spatial domain such as synthetic aperture radar (SAR) imaging, whereas in the second category, the images are sparse in a transform domain (e.g., CWD hologram imaging). In the second category, a transform domain such as Discrete Fourier Transform (DFT) or Discrete Cosine Transform (DCT), is required for image reconstruction. To reconstruct these sparse images from the hologram samples, various algorithms based on compressive sensing are used, such as the total variation (TV) minimization technique [10]. Moreover, the dictionary-learning-based methods are used to adaptively estimate a sparsity domain and reconstruct the image [11].

Another class of recovery methods consists of iterative methods, which repeatedly apply a simple recovery procedure. These methods are designed such that the signal of interest becomes the fixed-point of a transformation, and then, by repeatedly applying this transformation, an approximation of the fixed-point signal is improved. Hence, if the initial point is properly selected, the output gradually converges to the optimum solution. One of the advantages of the iterative methods is that even when the sampling scheme is not invertible, it still converges to a fair approximation of the desired outcome, while most interpolation-based methods diverge in such cases [12]. Iterative method with side information of spectral support is investigated in [13]. An iterative method with adaptive thresholding (IMAT) is introduced in [8], to reconstruct the sparse signals with sub-Nyquist rate. The IMAT algorithm is shown to work with both structured and random samples.
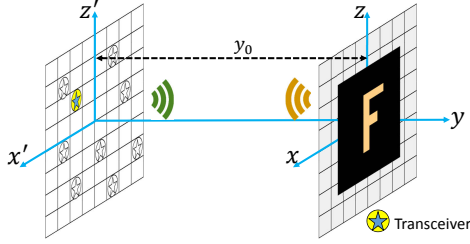
Fig. 1. Configuration of the mono-static imaging system.

In this paper, an imaging methodology based on random sampling and iterative hologram recovery for millimeter wave imaging systems is introduced. In this method, a random subset of the discretized points are selected. Therefore, the imaging process is very fast. Next, a tailored iterative algorithm is proposed to estimate the missing samples before recovering the image. Unlike [12], the proposed iterative method needs to solve a non-linear inverse problem.

This paper is organized as follows. In Section II the system model of a mono-static imaging device is presented. Then, the sparse imaging approach and the iterative recovery strategy are presented in Section III. The simulation and measured results and discussions are provided in Section IV. Finally, the paper is concluded in Section V.

II. SYSTEM MODEL

The mono-static imaging system is modeled as shown in Fig. 1, where the transceiver antenna elements measure the reflected signal from the object over a 2-D plane parallel to the object plane. Assume that the transceiver is located at $(x', 0, z')$ in x'-z' plane, while the point (x, y_0, z) in the object plane (x-z) is being scanned. If the reflected wave from $f(x, z)$ travels in a linear, isotropic, homogeneous, and non-dispersive medium, then, all components of the electric and magnetic fields are fully described by a single scalar wave equation [14]. The scattered field at the transceiver is a linear combination of the reflected waves from all the object points as stated in [15]. In practice, the scanner produces a finite number of samples. Hence, a discrete model for the imaging problem is required. The planes of the transceiver and the object are discretized into finite points. Let us consider the matrices $\mathbf{S}$ and $\mathbf{F}$ as the discretized planes of transceiver with $M \times N$ points, and the object plane with $P \times Q$ points, respectively. Then, s

$$\mathbf{S}[m, n] = \sum_{p=1}^{P} \sum_{q=1}^{Q} \mathbf{F}[p, q] \mathrm{e}^{-\mathrm{j}2kr[m,n,p,q]}, \quad (1)$$

where $r[m, n, p, q] = \sqrt{(m-p)^2 + y_0^2 + (n-q)^2}$ is the Euclidean distance between the transceiver position $[m, n]$ and the object point $[p, q]$. Moreover, k is the wavenumber. To estimate the hologram of the object, different approaches are presented in the literature such as [15], [9]. One common method is to use the generalized focusing technique (GSAFT) [15], which reconstructs the hologram as follows

$$f(x, z) = \mathscr{F}^{-1}\{\mathscr{F}\{s(x, z)\} \mathrm{e}^{-\mathrm{j}k_y y_0}\}, \quad (2)$$

where $k_y = \sqrt{4k^2 - k_x - k_z}$. The operators $\mathscr{F}\{\cdot\}$ and $\mathscr{F}^{-1}\{\cdot\}$ represent the 2-D Fourier transform and its 2-D

inverse, respectively. In this approach, the final estimated image is the absolute value of the inverse Fourier transform of phase shifted measurements in Fourier domain.

III. PROPOSED IMAGING METHOD

A. Recovery problem

In the conventional imaging approach, the transceiver scans the whole object uniformly with the Nyquist rate equal to $\lambda/2$ to avoid aliasing, where λ is the carrier wavelength. This approach is not time-efficient, since a large amount of samples is generated. On the other hand, usually the images are sparse in a transform domain, such as Fourier or Wavelet domains. Hence, the minimum number of the samples required to recover the sparse components is far less than the number of samples obtained from the uniform sampling. In addition, it is shown that the random sampling preserves the information of all components in the sparse domain. In this work, the Fourier domain is considered as the sparse domain and random sampling scheme by a known rate related to the number of sparse coefficients is used. The detail of the proposed imaging method is depicted in Fig. 2, where a random binary mask $(0/1)$ with the size of the discretized transceiver plane is used to reduce the processing samples. The transceiver follows the mask pattern and scans any point where its corresponding value is equal to 1. After scanning the object, a matrix of the measured hologram data is formed with missing points in matrix $(\mathbf{S}_s)$. The hologram data in this matrix belong to the spatial domain. To recover the missing samples of the hologram, the proposed algorithm is applied. Finally, the recovered hologram is processed using the GSAFT method to estimate the final image. In fact, a sparse matrix of data in Fourier domain is formed such that its projected samples in spatial domain are equal to the measured random samples. Mathematically, the following optimization problem is formed

$$\min_{\mathbf{S}'} \|\mathscr{F}\{\mathbf{S}'\}\|_0 \quad \text{subject to} \quad P_M(\mathbf{S}') = P_M(\mathbf{S}) \quad (3)$$

where $\| \cdot \|_0$ is the ℓ_0-norm, which is equal to the number of non-zero coefficients. $P_M(\cdot)$ is an operator with mask M (i.e. $P_M(\mathbf{S}) = M \odot \mathbf{S}$, where $\odot$ is the Hadamard product). Although (3) gives the desired solution, this is a non-deterministic polynomial time problem, which is computationally intensive. Hence, based on the theory of compressed sensing, the ℓ_0-norm is replaced by a sub-optimal convex relaxation approach, so the problem can be solved using ℓ_1-norm minimization [16], or

$$\min_{\mathbf{S}'} \|\mathscr{F}\{\mathbf{S}'\}\|_1 \quad \text{subject to} \quad P_M(\mathbf{S}') = P_M(\mathbf{S}) \quad (4)$$

The Basis Pursuit (BP) [17] and LASSO [18] algorithms are two common methods for solving problems similar to (4). In this paper, instead, an iterative algorithm is proposed, which is described in details in the following section.

B. Proposed Algorithm

To recover the hologram from its samples, an iterative method is employed, where its goal is to construct the inversion of the distortion operator by its samples [12]. The
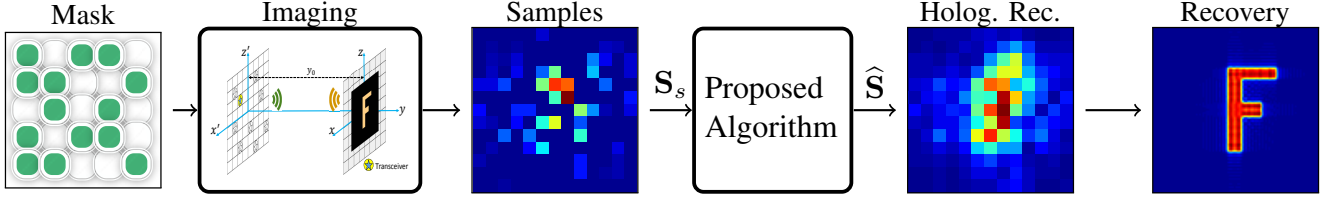
Fig. 2. Proposed imaging method. The green circles in Mask corresponds to the sampling points.
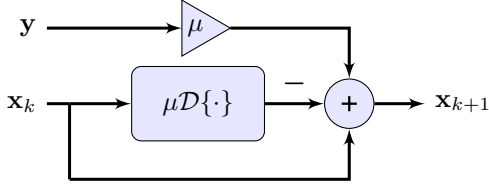

Fig. 3. The block diagram of the iterative method at $(k+1)$th iteration.

iterative recovery methods are tied to the fixed point theory in mathematics. The block diagram of the iterative recovery method is presented in Fig. 3. As it is shown, the process of signal recovery, $\mathbf{x}$, from its measured samples, $\mathbf{y}$, with distortion operator $\mathcal{D}\{\cdot\}$ at iteration $(k+1)$ is described by

$$\begin{cases} \mathbf{x}_{k+1} = \mathbf{x}_k + \mu\big(\mathbf{y} - \mathcal{D}\{\mathbf{x}_k\}\big) \\ \mathbf{y} = \mathcal{D}\{\mathbf{x}\} + \mathbf{n} \\ \mathbf{x}_0 = \mathbf{0} \end{cases}$$

where μ is the relaxation parameter and $\mathbf{n}$ is the noise vector.

Similar to the sparse recovery algorithms, the proposed approach is based on recovering the hologram iteratively. At each iteration, first the image is transformed into the Fourier domain (the sparsity domain). Next, the thresholding operator is applied to enforce the sparsity constraint, and then, the inverse Fourier transform is used to return to the pixel domain. Finally, the pixel values are replaced with the original values wherever available (the projection step). Hence, the operator $\mathcal{D}\{\cdot\}$ in the proposed algorithm consists of the thresholding step in the sparsity domain and replacing the measured samples in the pixel domain. By iteratively enforcing the sparsity constraint in the Fourier domain and the consistency constraint in the pixel domain, the missing samples are gradually recovered. In other words, after the iterative method converges, the recovered image satisfies both constraints. Thus, if the number of samples is sufficient to uniquely represent the image, the recovered image shall coincide with the original one. In other cases, the recovered image represents a sparse approximation of the original image. The block diagram of the proposed method is presented in Fig. 4. The thresholding operator $\mathcal{T}$ on matrix $\boldsymbol{X}$ with entries x_{ij} and threshold value τ is defined as

$$x_{ij} = 0 \text{ if } |x_{ij}| < \tau, \ x_{ij} = x_{ij} \text{ otherwise.} \tag{5}$$

Remark 1. To select the sparse components gradually, a suitable technique is to decrease the threshold level τ as the iteration number increases. Hence, an exponential threshold level is used

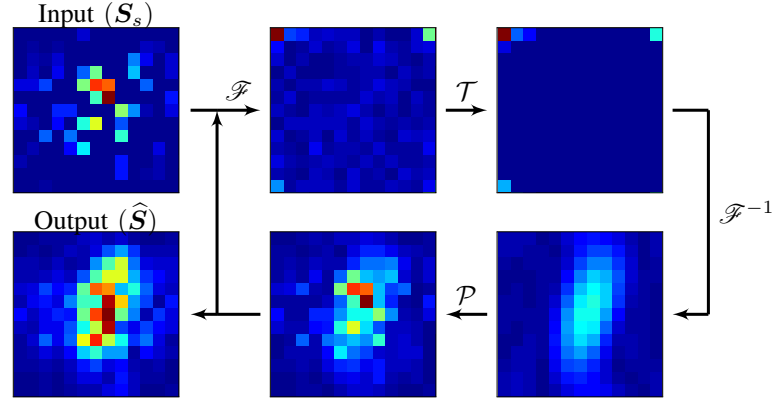$$\tau_k = \beta \mathrm{e}^{-\alpha k}, \tag{6}$$

Fig. 4. The block diagram of the proposed algorithm. The operators $\mathscr{F}$, $\mathcal{T}$, $\mathscr{F}^{-1}$, and $\mathcal{P}$ stand for the Fourier transform, the thresholding operator, the inverse Fourier transform and the projection operator, respectively.

TABLE I
THE RECONSTRUCTION PSNR IN dB AND THE SSIM METRIC FOR FIG. 5

Rate	5% (left col.)		20% (middle col.)		80% (right col.)	
Metric	PSNR	SSIM	PSNR	SSIM	PSNR	SSIM
GSAFT	12.12	0.0321	15.84	0.0730	21.28	0.1840
DMAS	12.64	0.0629	14.97	0.2799	19.28	0.8920
Proposed	16.01	0.0425	21.99	0.3295	23.62	0.8101

where $\beta = \|\mathscr{F}\{\boldsymbol{X}_0\}\|_\infty$, and $\alpha \in (0,1)$. Parameter β is set to the largest coefficient to assure that there is at least one coefficient to be picked up in the first iteration.

The projection operator, which maps the measured samples to their locations is

$$\mathcal{P}_M\{\boldsymbol{S}_s, \boldsymbol{Z}\} = \boldsymbol{S}_s + (1 - \boldsymbol{M}) \odot \boldsymbol{Z}, \tag{7}$$

The projection $\mathcal{P}_M\{\boldsymbol{S}_s, \boldsymbol{Z}\}$ returns a matrix, whose entries are selected from $\boldsymbol{Z}$ (the IFFT of (5)) if the corresponding entries in $\boldsymbol{M}$ are zero, otherwise they are selected from $\boldsymbol{S}_s$. The algorithm terminates when the relative variation of the reconstructed images between the two consecutive iterations is smaller than ϵ. The parameter ϵ is determined empirically.

IV. SIMULATION AND EXPERIMENTAL RESULT

In this section, the proposed method is examined and compared with the conventional methods such as GSAFT [15], FFT-SAR [19], and delay multiply and sum (DMAS) [20]. The mono-static imaging system operates at 30 GHz, so the minimum sampling space is $\lambda/2 = 0.5$ cm. The distance between the transceiver and object planes is equal to 100 cm. Also, both planes are discretized to 100×100 grid points. The threshold decay factor is set to $\alpha = 0.1$. To have a fair comparison, the structural similarity index measure (SSIM)

(a) (b)

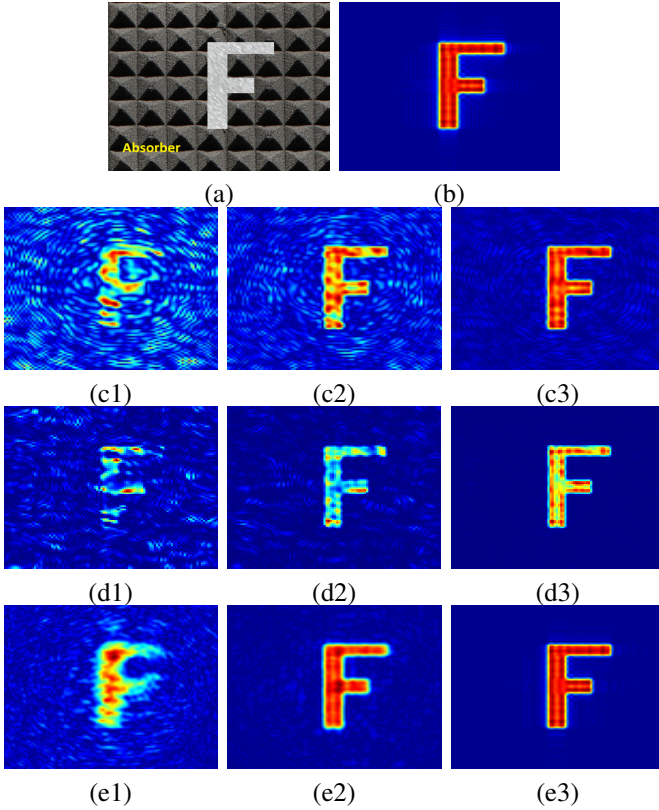(c1) (c2) (c3)

(d1) (d2) (d3)

(e1) (e2) (e3)

Fig. 5. Reconstruction of "F" shape for different sampling rates. (a) Object, (b) full scan result. Recovery using (c) GSAFT, (d) DMAS, and (e) the proposed method. The reconstruction PSNR in dB and the SSIM metric are shown in Table I.

metric [21] and the peak signal-to-noise ratio (PSNR) metric of the reconstructed images are calculated for each reconstructed image, where the full scan reconstruction is considered as the benchmark. The PSNR value considering the benchmark $\mathbf{F}_{M \times N}$ and the estimated images $\widehat{\mathbf{F}}$ is derived from

$$\text{PSNR(dB)} = 10 \log_{10} \left(\frac{\max(\mathbf{F})^2}{\left(\sqrt{\sum_{i,j} (\mathbf{F}_{i,j} - \widehat{\mathbf{F}}_{i,j})^2} \right) / (MN)} \right). \quad (8)$$

For the first simulation, the synthetic image of the shape F, depicted in Fig. 5(a), is used. Fig. 5(b) shows the full scan reconstruction as the benchmark for comparison. A random mask is generated with different sparsity rates. The measured samples with rates of 5%, 20%, and 80% with respect to the full scan are fed to the GSAFT, DMAS and the proposed method. The recovered images are shown in Fig. 5. Due to the sparsity of the image, the proposed method successfully estimates the image. Specifically, recovery with only 20% of samples reconstructs a high quality image with PSNR of 21.99 dB, which is higher than the case when 80% of the samples are recovered directly by GSAFT method. In the second simulation, the sampling rate is varied from 10% to 90% with the step size of 10%, and calculate the PSNR and SSIM of five methods: GSAFT, linear interpolation for the missing sample recovery, FFT-SAR, DMAS and the proposed method. Figure 6 shows that by using the proposed algorithm, even with under-sampling, a high-quality reconstruction is performed. In particular, in the case of 30% sampling rate with the proposed method, almost the same quality as the case of 90% sampling rate with GSAFT method is obtained.
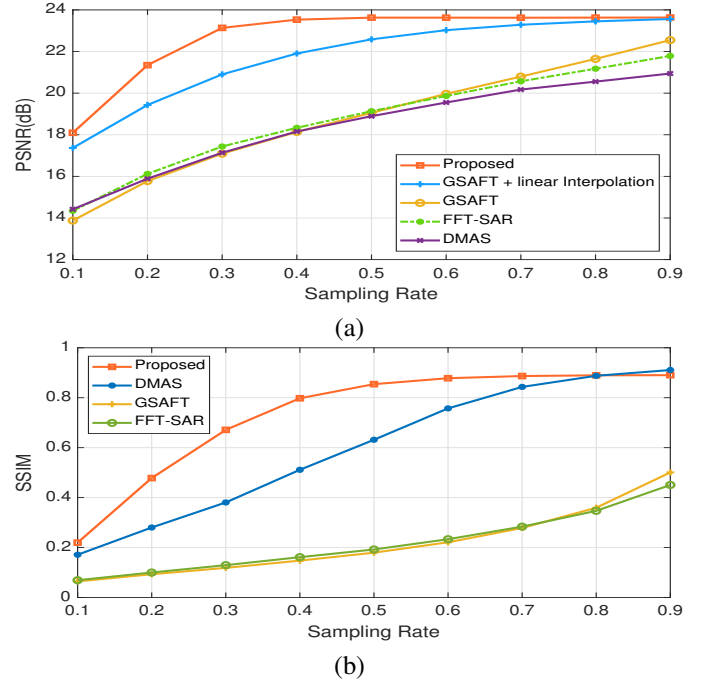

(a)

(b)

Fig. 6. Reconstruction quality of random sampling versus sampling rate for F shape (Fig. 5(a)), (a) PSNR metric, (b) SSIM metric.
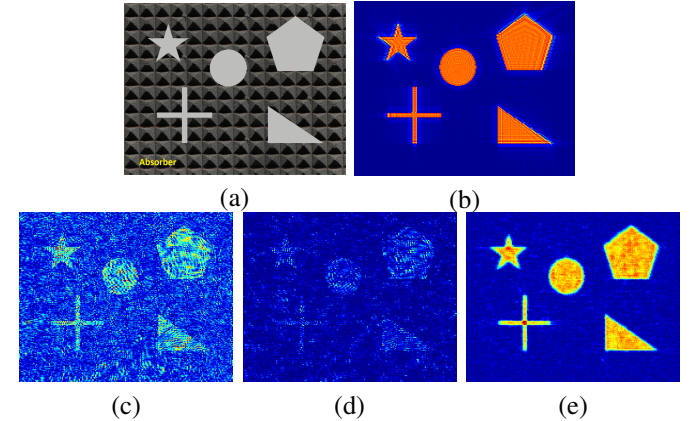

(a) (b)

(c) (d) (e)

Fig. 7. A scene with multiple shape objects scanned with 20% undersampling. (a) Complex resolution chart, (b) full scan, (c) GSAFT, PSNR: 12.57dB (SSIM= 0.0325), (d) DMAS, PSNR: 9.52dB (SSIM= 0.0567), (e) proposed PSNR: 17.31dB (SSIM= 0.1365).

In the third test, several complex shapes with low sparsity are employed to study the performance of the proposed algorithm. For more complex shapes, the sparsity of the image decreases, therefore, more samples are required for better reconstruction. The complex resolution chart with size of 200×200 points and the simulation results for the sampling rate of 20% are depicted in Fig. 7. These results state that the proposed method successfully recovers the image with PSNR of 17.31 dB (SSIM = 0.1365), which is about 5 dB higher than that of the GSAFT recovery method.

In the last experiment, the proposed methodology is applied to the practical data obtained by the system illustrated in Fig. 8. The imaging system consists of two horn antennas with 20 dB gain at Ka-band ($26.5 - 40$ GHz) used as TX and RX antennas, an RF amplifier with 18 dB gain and a mechanical positioner, which moves the antennas to scan the object in Cartesian plane. The TX and RX antennas are
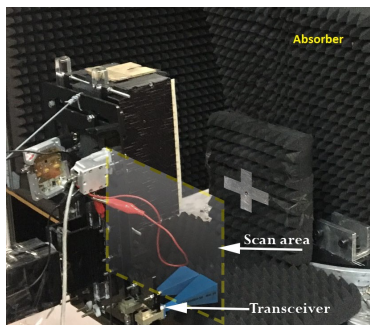
Fig. 8. Practical setup for imaging at 30 GHz. The shape is parallel to the transceiver plane.
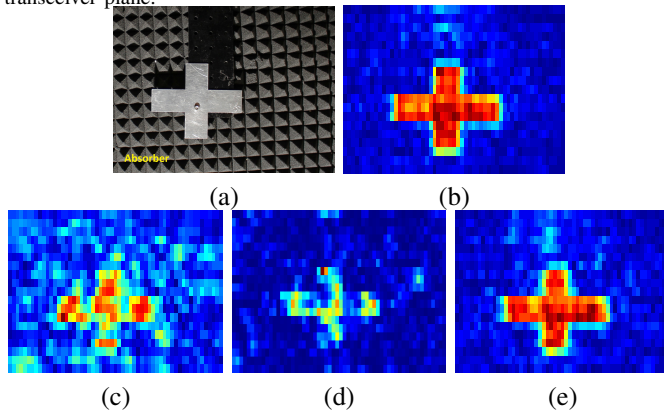

Fig. 9. Measurement results. (a) Original object, (b) full scan, (c) GSAFT with 40% sampling rate, PSNR: 14.25 dB (SSIM= 0.2424), (d) DMAS with 40% sampling rate, PSNR: 13.67dB (SSIM= 0.2596), (e) proposed method with 40% sampling rate, PSNR: 25.02dB (SSIM = 0.6583).

connected to HP8722ES network analyzer, which transmits and receives millimeter-wave signals. The whole system is placed inside an anechoic chamber, where undesired reflectors are absorbed. The distance between the transceiver and object planes is 30 cm. The horn antennas follow the binary mask of size 55×55 for imaging. The scanning time at each sensor node (essentially each pixel) takes 0.1 ms. The measured received signal is saved in the computer and then the proposed algorithm is applied. The sampling rate of 40% is used in this experiment, where a metal cross object is used. The results are depicted in Fig. 9. The proposed method successfully reconstructs the image from a subset of samples with a PSNR of 25.02 dB.

The execution time of the proposed algorithm on images size of 100×100 is measured as 35.1 ms on average over 1000 independent runs with varying sampling rates. For a typical case, consider a 30% undersampling rate which translates into dropping 3000 pixels. This saves us 300 ms of scanning time, while our method adds 35.1 ms to the overall computation time. The algorithm was implemented in MATLAB 2019b on a workstation with Intel(R) Core(TM) i7-4930K CPU @3.40 GHz(12 CPUs) and 16 GB RAM. On this workstation for the sampling rate of 20% the execution time of reconstruction process for GSAFT, proposed approach, and DMAS are 3.12 sec, 3.39 sec and 97.70 sec, respectively.

V. CONCLUSION

In this paper, an imaging methodology for the mono-static millimeter wave systems was introduced, based on random sampling with the specific rates related to the sparsity of the hologram in a transform domain. To achieve a high resolution recovery, an iterative algorithm is proposed to recover the missing samples of the hologram. Simulation results on the synthetic shapes as well as the experimental data proved the successful performance of the proposed imaging and recovery methods. For example, it was shown that by using only 20% of the regular samples, the imaging process is performed faster. Furthermore, the achieved PSNR in the reconstruction is over 20 dB, which is higher than the case where 80% of samples are processed with the direct GSAFT method.

REFERENCES

[1] S. S. Ahmed *et al.*, "A Novel Fully Electronic Active Real-Time Imager Based on a Planar Multistatic Sparse Array," *IEEE Trans. Microw. Theory Tech.*, vol. 59, no. 12, pp. 3567–3576, 2011.

[2] T. S. Rappaport *et al.*, "Wireless communications and applications above 100 ghz: Opportunities and challenges for 6g and beyond," *IEEE Access*, vol. 7, pp. 78 729–78 757, 2019.

[3] M. C. Kemp, "Millimetre wave and terahertz technology for detection of concealed threats - a review," in *2007 Joint 32nd International Conference on Infrared and Millimeter Waves and the 15th International Conference on Terahertz Electronics*, 2007, pp. 647–648.

[4] H. Van Trees, *Detection, Estimation, and Modulation Theory, Optimum Array Processing*. Wiley, 2002.

[5] T. E. H. David M. Sheen, "Reconstruction techniques for sparse multi-static linear array microwave imaging," *Proc.SPIE*, vol. 9078, 2014.

[6] M. Kazemi *et al.*, "Spectral redundancy compensation in multi-static millimeter-wave imaging," *IEEE Trans. on Circuits and Systems II: Express Briefs*, vol. 65, no. 5, pp. 687–691, May 2018.

[7] H. Zamani and M. Fakharzadeh, "1.5-d sparse array for millimeter-wave imaging based on compressive sensing techniques," *IEEE Trans. on Antennas and Propagation*, vol. 66, no. 4, pp. 2008–2015, April 2018.

[8] F. Marvasti and *et al.*, "A unified approach to sparse signal processing," *EURASIP Journal on Advances in Signal Processing*, vol. 2012, no. 1, p. 44, Feb 2012.

[9] Q. Cheng, A. Alomainy, and Y. Hao, "Compressive millimeter-wave phased array imaging," *IEEE Access*, vol. 4, pp. 9580–9588, 2016.

[10] Y. Wang, J. Yang, W. Yin, and Y. Zhang, "A new alternating minimization algorithm for total variation image reconstruction," *SIAM Journal on Imaging Sciences*, vol. 1, no. 3, pp. 248–272, 2008.

[11] C. Jiang, Q. Zhang, R. Fan, and Z. Hu, "Super-resolution ct image reconstruction based on dictionary learning and sparse representation," *Scientific reports*, vol. 8, no. 1, p. 8799, 2018.

[12] A. Amini and F. Marvasti, "Convergence analysis of an iterative method for the reconstruction of multi-band signals from their uniform and periodic nonuniform samples," *Sampling Theory in Signal and Image Processing (STSIP)*, vol. 7, no. 2, pp. 109–112, 2008.

[13] F. Marvasti, "Spectral analysis of random sampling and error free recovery by an iterative method," *Transactions of IECE of Japan. Section E*, vol. 69, no. 2, pp. 79–82, 1986.

[14] J. W. Goodman, *Introduction to fourier optics*. McGraw-Hill, 1996.

[15] D. M. Sheen, D. L. McMakin, and T. E. Hall, "Three-dimensional millimeter-wave imaging for concealed weapon detection," *IEEE Trans. Microw. Theory Tech.*, vol. 49, no. 9, pp. 1581–1592, 2001.

[16] E. J. Candes, J. K. Romberg, and T. Tao, "Stable signal recovery from incomplete and inaccurate measurements," *Communications on pure and applied mathematics*, vol. 59, no. 8, pp. 1207–1223, 2006.

[17] S. S. Chen, D. L. Donoho, and M. A. Saunders, "Atomic decomposition by basis pursuit," *SIAM review*, vol. 43, no. 1, pp. 129–159, 2001.

[18] R. Tibshirani, "Regression shrinkage and selection via the lasso," *Journal of the Royal Statistical Society: Series B (Methodological)*, vol. 58, no. 1, pp. 267–288, 1996.

[19] M. Soumekh, "A system model and inversion for synthetic aperture radar imaging," *IEEE Trans. on Image Proc*, vol. 1, no. 1, pp. 64–76, Jan 1992.

[20] H. Been Lim, N. Thi Tuyet Nhung, E. Li, and N. Duc Thang, "Confocal microwave imaging for breast cancer detection: Delay-multiply-and-sum image reconstruction algorithm," *IEEE Transactions on Biomedical Engineering*, vol. 55, no. 6, pp. 1697–1704, June 2008.

[21] Zhou Wang *et al.*, "Image quality assessment: from error visibility to structural similarity," *IEEE Trans. on Image Processing*, vol. 13, no. 4, pp. 600–612, April 2004.